1 *Manuscript for*

Source-Dependent Optical Properties and Molecular Characteristics of Atmospheric Brown Carbon

4 **Authors**: Jinghao Zhai[1,3], Yin Zhang[1,2], Pengfei Liu[4], Yujie Zhang[1,2], Antai Zhang[1,2], Yaling

5 Zeng[1,2], Baohua Cai[1,2], Jingyi Zhang[1,2], Chunbo Xing[1,2], Honglong Yang[5], Xiaofei Wang[3],

6 Jianhuai Ye[1,2], Chen Wang[1,2], Tzung-May Fu[1,2], Lei Zhu[1,2], Huizhong Shen[1,2] , Shu Tao[1,2], Xin

7 Yang[1,2]*

8 *[1]Shenzhen Key Laboratory of Precision Measurement and Early Warning Technology for Urban*

9 *Environmental Health Risks, School of Environmental Science and Engineering, Southern*

10 *University of Science and Technology, Shenzhen 518055, China*

11 *[2]Guangdong Provincial Observation and Research Station for Coastal Atmosphere and Climate*

12 *of the Greater Bay Area, Shenzhen 518055, China*

13 *[3]Shanghai Key Laboratory of Atmospheric Particle Pollution and Prevention (LAP[3]), Department*

14 *of Environmental Science and Engineering, Fudan University, Shanghai 200438, China*

15 *[4]School of Earth and Atmospheric Sciences, Georgia Institute of Technology, Atlanta, GA 30332,*

16 *USA*

17 *[5]Shenzhen National Climate Observatory, Meteorological Bureau of Shenzhen Municipality,*

18 *Shenzhen 518040, China*

19

20 *To whom correspondence should be addressed.

21 Correspondence to: Xin Yang

22 Email: yangx@sustech.edu.cn

ABSTRACT: Atmospheric brown carbon (BrC) can significantly affect Earth's radiation budget by its wavelength-dependent absorption in the ultraviolet (UV)-visible range. BrC consists of a wide variety of organics with different optical properties, making accurate climate modeling essential for understanding its radiative impact. Here, we conducted a field campaign during the summer in Shenzhen, China, to investigate the optical properties and molecular characteristics of BrC from diverse particle sources using both online and offline measurements. Different sources of BrC, including those from secondary production associated with ozone pollution, urban transportation, and biomass burning, were identified through meteorological data and particle chemical compositions. The results show that the mass absorption cross-section (MAC) of BrC varied across sources, with BrC from biomass combustion exhibiting the highest MAC at 370 nm (3.42 ± 0.41 m^2/g) and secondary BrC associated with ozone pollution showing the lowest (1.25 ± 0.56 m^2/g). Nevertheless, secondary BrC exhibited the highest absorption Ångström exponent (AAE) while the BrC from biomass burning had the lowest AAE. Molecular analysis revealed that species in the CHON family from biomass burning demonstrated the strongest light absorption. Our results provide valuable insights for quantifying the source-specific optical properties of BrC, enhancing the accuracy of climate models.

Graphical abstract
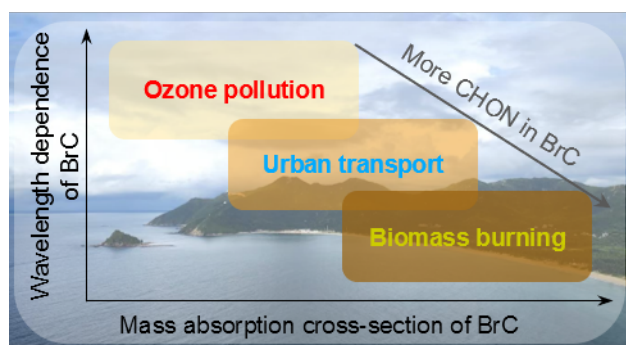
1 INTRODUCTION

Atmospheric light-absorbing organic aerosols, known as brown carbon (BrC), are important contributors to the global radiation absorption of atmospheric aerosols, alongside black carbon (BC). The absorption properties of BrC are wavelength-dependent, with relatively weak absorption in the mid- and long-visible wavelengths and a pronounced increase in absorption toward the short-visible and near-ultraviolet (UV) wavelengths (Sun et al., 2007;Laskin et al., 2015). Atmospheric BrC is primarily generated from the combustion of biomass and biofuels, as these processes typically occur under relatively low-temperature, fuel-rich conditions, which promote the formation of organics (Saleh et al., 2014;Chen and Bond, 2010). Additionally, secondary reactions in the atmosphere also play a significant role in the production of BrC (Laskin et al., 2015;Moise et al., 2015). It has been observed that BrC can be formed in secondary organic aerosols (SOA) through the nitration of volatile organic compound (VOC) precursors (Zhong and Jang, 2011;Lambe et al., 2013;Updyke et al., 2012;Haynes et al., 2019), aqueous-phase reactions of ammonia or amino acids with carbonyl-containing SOA (Updyke et al., 2012;Flores et al., 2014;Zarzana et al., 2012), and bond-forming reactions among SOA constituents that generate dimers and larger oligomers (Shapiro et al., 2009;Bones et al., 2010;Chang and Thompson, 2010). Unlike BC, which exhibits relatively uniform physicochemical properties, BrC comprises a broad spectrum of light-absorbing organic species, resulting in large variability in its optical properties (Updyke et al., 2012;Saleh et al., 2018). To accurately assess the radiative impacts of BrC, its diverse properties must be effectively represented in climate models.

Aerosol light absorption can be quantified using the mass absorption cross-section (MAC), a key parameter that links radiative transfer to aerosol mass in climate models (Bond and Bergstrom, 2006). MAC can be calculated from measurements of aerosol light absorption coefficient and mass concentration. The absorption Ångström exponent (AAE) describes the wavelength dependence of aerosol light absorption. For BC aerosols, AAE values are typically close to 1 (Bond and Bergstrom, 2006). In contrast, BrC shows substantial variability in wavelength dependence, with AAE values ranging from 2 to as high as 11 (Laskin et al., 2015). The optical properties of BrC

are highly source-dependent (Saleh et al., 2014;Kumar et al., 2018). Moreover, BrC absorption evolves dynamically during atmospheric aging through processes like photobleaching or photo-enhancement, leading to uncertainties in the quantification of the radiative effects of atmospheric aerosols (Wong et al., 2017;Sumlin et al., 2017;Li et al., 2020).

The measurement of the optical properties of BrC is crucial for accurately determining its role in global radiation balance. In filter-based offline analysis, the optical properties of a bulk film can be measured using an ultraviolet-visible (UV-vis) spectrometer (Zhong and Jang, 2011). While the varying solubility of BrC components in different solvents could introduce uncertainties in offline analyses (Shetty et al., 2019), solvent-induced chemical artifacts, particularly those associated with methanol extraction, have also been shown to significantly alter the optical properties of BrC (Kumar et al., 2018;Saleh et al., 2014). Therefore, online MAC measurements provide a more consistent and reliable benchmark, and integration with carefully selected offline extractions can offer a more comprehensive understanding of the relative abundance of BrC classes (Chen et al., 2022b). Nevertheless, the optical properties of BrC retrieved from online measurements can be subject to biases due to the limitations of the techniques employed. For example, transmission measurements through aerosol-laden filters have been used to quantify aerosol absorption properties (Petzold et al., 2005;Bond and Bergstrom, 2006). These approaches usually assume that aerosol particles retain their morphology upon adhering to the filters, potentially leading to uncertainties in the interpretation of filter absorption data (Subramanian et al., 2007). Various online approaches have been developed to directly measure the absorption, scattering, and extinction coefficients of aerosols, either independently or in combination. Cavity-based techniques offer highly sensitive and accurate measurements of the overall extinction coefficient (Riziq et al., 2007;Massoli et al., 2010). An integrating nephelometer enables the independent measurement of the scattering coefficient (Anderson and Ogren, 1998;Bond et al., 2009). Photoacoustic instruments are widely recognized for providing accurate absorption measurements (Arnott et al., 1998;Lewis et al., 2008). Studies comparing photoacoustic and filter-based methods

indicate that filter-based techniques often overestimate absorption, although the AAE derived from both methods generally aligns more closely (Al Fischer and Smith, 2018;Saleh et al., 2014).

The complex chemical composition of BrC leads to significant variability in its optical properties. The molecular characteristics of BrC components vary based on their sources, making specific molecular information valuable for source attribution. Studies have shown that the molecules responsible for BrC absorption in biomass burning aerosols tend to be large and highly unsaturated (Sun et al., 2007). Nitroaromatics, primarily including nitro-substituted benzene, pyrrole, naphthalene, and indole derivatives, are commonly identified as BrC chromophores (Jiang et al., 2019;Mayorga et al., 2022;Baboomian et al., 2023;Cui et al., 2024;Dalton et al., 2024), which are either directly emitted from biomass burning or formed through atmospheric reactions involving combustion products, nitrogen oxides, or nitrous acid (Li et al., 2014;Chen et al., 2011;Desyaterik et al., 2013). Amines, another group of nitrogen-containing compounds, are often detected in BrC, where they frequently serve as reactants in the formation of SOA (Nozière et al., 2009). High-resolution mass spectrometry (HRMS) has been widely used for offline characterization of BrC to obtain detailed molecular-level information. To improve detection accuracy, BrC components are often separated using chromatography before MS analysis, allowing for more precise molecular identification (Claeys et al., 2012;Zhang et al., 2013;Desyaterik et al., 2013). To fully understand how the chemical variability of BrC influences atmospheric radiation, it is crucial to conduct detailed chemical analyses of BrC and incorporate the updated BrC classifications into the climate models.

Previous studies on BrC have mostly been based on laboratory simulations of typical sources, whereas field-based measurements involving multiple BrC sources remain limited. This is partly due to the inherent difficulty of distinguishing contributions from different sources under complex ambient conditions, especially when using bulk sampling methods. In light of these challenges, we adopted a case-based analysis framework to explore how different dominant source regimes and meteorological scenarios affect the optical properties of BrC in real-world settings. In this study, we conducted a field campaign during the summer of 2022 at Xichong site (22.48ºN, 114.56ºE),

122   located on the Dapeng Peninsula of Shenzhen, China. Particle optical properties and chemical

123   compositions were measured both online and offline. Different sources of BrC were identified

124   through meteorological data and the chemical compositions of particles. The optical properties of

125   BrC from different sources were evaluated and compared, supported by molecular

126   characterizations. Our study provides direct observational evidence of varying BrC sources with

127   different optical properties in the ambient, contributing to a deeper understanding of BrC's

128   radiative effects in climate models.

129   **2 METHODS**

130   **2.1 Field Measurements**

131   Field measurements were conducted at Xichong site (22.48°N, 114.56°E, Figure S1) on the Dapeng

132   Peninsula in Shenzhen, China, from August to September 2022. The analysis period used in this

133   study was from 27 August to 9 September 2022, corresponding to the overlapping operation time

134   of all deployed instruments. Located about 60 km from the city center, Xichong site is surrounded

135   by the sea and distant from urban areas and industrial sources, with over 90% forest coverage. Due

136   to minimal local anthropogenic interference, Xichong site serves as a regional atmospheric

137   background station in South China.

138   During the field campaign, an aethalometer (AE31, Magee Scientific, USA) operating at seven

139   wavelengths (370, 470, 520, 590, 660, 880, and 950 nm) and a photoacoustic extinctiometer (PAX,

140   Droplet Measurement Techniques, USA) measuring at 532 nm, were utilized to detect the online

141   optical properties of particles. A Monitor for AeRosols and Gases in Ambient air (MARGA,

142   Metrohm-Applikon, Netherlands) was conducted to detect the online water-soluble ion

143   concentration (NH_4^+, Na^+, K^+, Ca^{2+}, Mg^{2+}, SO_4^{2-}, NO_3^-, Cl^-). Detailed information regarding the

144   instrumentation and measurement uncertainties of the aethalometer is provided in the Supporting

145   Information (SI, Text S1). In this study, the time resolution of all online data was standardized to

146   1 h. Offline filter sampling was also carried out simultaneously during the field campaign. A high-

147   volume sampler (XT1025, XTrust Analytical Instruments, China) with a flowrate of $1m^3$/min was

148   used to collect PM$_{2.5}$ samples on the pre-baked quartz filters with sampling period of 24 h for each

149   filter. Details on the filter pretreatment procedures are available in the SI (Text S2). The filters

150   were further analyzed to measure the BrC mass, optical properties, and molecular characteristics.

151   Other measurements including the mass concentration of PM$_{2.5}$, O$_3$, and the meteorological

152   factors (temperature, relative humidity, wind speed, and wind direction), were conducted at the

153   sampling site. The HYSPLIT-4 (Hybrid Single-Particle Lagrangian Integrated Trajectory) model

154   developed by the ARL (Air Resources Laboratory) of the NOAA (National Oceanic and

155   Atmospheric Administration, USA) was employed to compute 24 h air mass back trajectories at a

156   50 m arrival height.

157   **2.2 Mass absorption cross-section of BrC**

158   The mass absorption cross-section (MAC, m^2/g) of BrC can be calculated according to the

159   following equation:

160$$\mathrm{MAC}(\lambda) = \frac{b_{\mathrm{abs,BrC}}(\lambda)}{[\mathrm{BrC}]} \tag{1}$$

161   where $b_{\mathrm{abs,BrC}}(\lambda)$ is the light absorption coefficient (Mm^{-1}) of BrC at a given wavelength λ,

162   derived by subtracting the corresponding absorption coefficient of BC from the total particle

163   absorption coefficient. Here, we used both online and offline methods to calculate the MAC of

164   BrC.

165   **2.2.1 Online determination of BrC light absorption coefficient and MAC calculation**

166   Previous studies have reported that the b_{abs} estimated from the aethalometer is generally larger

167   than that measured by the PAX, likely due to artifacts associated with organic matter loading on

168   the filter (Lack et al., 2008;Cappa et al., 2008;Saleh et al., 2014). In this study, the correlation

169   between the b_{abs} derived from the aethalometer ($b_{\mathrm{abs,520}}$) and the PAX ($b_{\mathrm{abs,532}}$) is shown in

170   Figure S2. The aethalometer-derived b_{abs} were scaled by a factor of 2 across all wavelengths for

171   subsequent MAC calculations. We consider the light absorption coefficient at a wavelength of 880

172   nm detected by the aethalometer to be primarily attributed to BC, with minimal contribution from

BrC absorption (Laskin et al., 2015). Based on the fact that BC has minimal wavelength dependence, with an AAE of ~1 (Bond and Bergstrom, 2006), the BC absorption coefficient at wavelength λ, $b_{abs,BC}(\lambda)$, is given by:

$$b_{abs,BC}(\lambda) = b_{abs,BC}(880) \times (\frac{\lambda}{880})^{-1} \tag{2}$$

And thus the $b_{abs,BrC}(\lambda)$ is calculated by:

$$b_{abs,BrC}(\lambda) = b_{abs}(\lambda) - b_{abs,BC}(\lambda) \tag{3}$$

The light absorption coefficients of the aethalometer were not directly measured but were converted and corrected (Text S1). In this study, we focus on wavelengths of 370 nm and 550 nm for all the optical measurements, representing the high light absorption band and mid-visible band of BrC, respectively, to facilitate comparisons with results from other studies. Thus, the absorption coefficient at 520 nm wavelength detected by the aethalometer was converted to 550 nm using the following equations:

$$b_{abs}(550) = b_{abs}(520) \times (\frac{550}{520})^{-AAE_{370-550}} \tag{4}$$

$$AAE_{370-550} = -\frac{ln[b_{abs}(370)] - ln[b_{abs}(550)]}{ln(370) - ln(550)} \tag{5}$$

2.2.2 Offline determination of BrC mass concentration and MAC calculation

In equation (1), [BrC] is the mass concentration of BrC. Since BrC is fundamentally an optical concept, the optical-equivalent mass of BrC can be determined according to the absorption coefficient of BrC by assuming its MAC. Currently, there is no unified method for the direct measurement of BrC mass. Commonly used methods for characterizing BrC include thermal desorption and dissolution methods for characterization of BrC mass, although both come with inherent uncertainties. The thermal desorption method quantifies BrC mass by heating the volatile OC of the particle, taking advantage of the lower volatilization point of BrC than BC (Massabò et al., 2016;Olson et al., 2015;Pani et al., 2021). However, it may also include some non-absorbing OC and may induce pyrolysis during the heating process, which brings further uncertainties into

8

197   the measurement. The dissolution method measures the BrC mass after extraction in the solvent

198   (water, methanol, acetone, etc.) (Rathod et al., 2024). Nevertheless, some BrC may not be soluble,

199   which carries uncertainties to the dissolution method.

200   In this study, we used both thermal desorption and dissolution methods to measure the $[BrC]$.

201   For the thermal desorption method, the BrC mass was measured using an organic carbon/elemental

202   carbon analyzer (OC/EC analyzer, DRI 2015, Magee Scientific, USA) based on the filter samples.

203   Detailed information on the OC/EC analyzer mechanism is provided in the SI (Text S3). The

204   temperature-separated carbon fractions from aerosol filter deposits were quantified for the mass

205   concentration of OC that evaporated up to $580^{\circ}C$ ($[OC_T]$), which was taken as a representative of

206   the BrC mass concentration to calculate the MAC.

207   During the campaign, the optical measurement function of the OC/EC analyzer was

208   malfunctioning. The $b_{abs,BrC}$ values were based on online data from the aethalometer ($b_{abs,AE31}$)

209   with one data point per hour, whereas the $[OC_T]$ values were derived from offline filter sampling

210   with one data point every 24 hours. To align the temporal resolution of the data, we used $[OC_T]$

211   relative to the total particulate mass (PM_{filter}) on each filter (every 24 hours) as a fixed ratio. This

212   ratio was then applied to the hourly $PM_{2.5}$ mass concentration ($[PM_{2.5}]$) over the corresponding

213   24-hour period, yielding the calculated hourly BrC mass concentration as given by equation (3).

214   There might be limitations arising from the fixed BrC mass ratio ($\frac{[OC_T]}{[PM_{filter}]}$) used to calculate the

215   MAC over 24 hours, as the time resolution differs from the hourly $b_{abs,AE31}$. However, we believe

216   that the quantification of BrC mass in this study does rely on the offline filter-based analysis. The

217   time resolution of the online $MAC_{BrC,\lambda}$ in this study is one hour.

$$MAC_{BrC,\lambda} = \frac{b_{abs,AE31}(\lambda)}{\frac{[OC_T]}{[PM_{filter}]} \times [PM_{2.5}]} \qquad (6)$$

218

219   Meanwhile, we measured the mass concentration and light absorption of water-soluble organic

220   carbon (WSOC). The solubility of BrC varies across different solvents. However, in this study, the

221   mass concentration of WSOC ($[WSOC]$) was chosen for the calculation of MAC, and BrC

dissolved in other solvents was not further discussed. The sample filters were stored at -20 °C prior to analysis. Each filter was ultrasonically extracted in deionized water at room temperature, and the original extract was directly used for absorbance measurements. The mass concentration of WSOC in the collected filter samples was measured using a total organic carbon analyzer (TOC analyzer, N/C 3100, Analytik Jena, Germany). We further compared the $[OC_T]$ detected by the thermal desorption method and the [WSOC] measured by the dissolution method (Figure S3), which showed good correlation (r^2=0.844) while the $[OC_T]$ was more than twice of the [WSOC].

The light absorption of WSOC was further measured using an ultraviolet- visible (UV-vis) spectrometer (T2600, York Instrument, China) within the wavelength ranging from 190 to 1100 nm. The WSOC light absorption was then converted into light absorption coefficients ($b_{abs,WSOC}$), as given by equation (4):

$$b_{abs,WSOC}(\lambda) = \ln(10) \times (A_\lambda - A_{880}) \times \frac{V_l}{V_a \times L} \tag{7}$$

where A_{880} is the systematic baseline drift, V_l (m^3) is the volume of water (30 mL) used for extraction, V_a (m^3) is the volume of the sampled air, and L (cm) is the optical path length of the quartz cuvette (1 cm) in the UV-vis spectrometer. The filter-based offline $MAC_{WSOC,\lambda}$ is calculated according to:

$$MAC_{WSOC,\lambda} = \frac{b_{abs,WSOC}(\lambda)}{[wsoc]} \tag{8}$$

The MAC values reported in this study were calculated based on measured OC concentrations, derived from both an online aethalometer and offline WSOC analysis. As these methods are carbon-specific, using OC as the mass basis ensures consistency across the dataset.

2.3 Chemical molecular analysis

A high-performance liquid chromatography (HPLC) equipped with a photodiode array (PDA, G7117C, Agilent, USA) detector and a high-resolution mass spectrometer system (HRMS, G6545A, Agilent, USA) was utilized to identify the molecular composition, determine the relative

abundance, and measure the corresponding light absorption of BrC. The HPLC was equipped with a C18 column (EC-C18, 3×150 mm, 2.7 µm particles, Agilent, USA), using mobile phases of 0.1% formic acid-water (A, HPLC grade) and 0.1% formic acid-acetonitrile (B, HPLC grade). Gradient elution for each sample was performed with the A-B mixture as: 0~1 min hold at 95% A, 1~20 min linear decreased to 5% A, 20~27 min hold at 5% A, and then 27~30 min hold at 95% A. The HRMS was set with a soft electrospray ionization source (ESI) in full scan, operating in both positive and negative ion modes. Raw data from mass spectrometry were processed using MassHunter Qualitative Analysis (v10.0). Molecule concentrations were semi-quantified based on the intensity from mass spectrometry (Kruve, 2019;Zhang et al., 2023).

The absorbance of the PDA at 370 nm was selected as the intensity of light absorption of BrC (Hecobian et al., 2010;Wen et al., 2021). Using a peak extraction algorithm in MassHunter Qualitative Analysis, approximately 20 absorption peaks per sample were identified. The absorption intensity at a specific retention time was determined by subtracting the blank absorption from the sample absorption. Peaks were grouped by overlapping retention times, with molecules in each group recorded along with their absorbance detected by the PDA. We employed a partial least squares regression (PLSR) model to attribute individual molecular absorbance (Text S4), clarifying the relationship between absorbing molecules and the absorbance of individual peaks (Zhang et al., 2023).

3 RESULTS AND DISCUSSION

3.1 Light absorption of BrC from different sources

During our sampling period, wind at the Xichong site predominantly came from two directions: northwest and northeast (Figure 1a, Figure S4). Air masses from the northwest primarily originated from inland areas of the peninsula, while those from the northeast were from the sea (Figure S1). High ozone levels were observed at times, mainly during the daytime, and were associated with relatively high nitrate concentrations (Figures 1b & 1c). Additionally, water-soluble potassium, as a marker for biomass-combusted aerosols (Zhai et al., 2015), also exhibited a time of elevated

levels during our observation (Figure 1c). Based on distinct meteorological and pollutant concentration characteristics, we selected three typical cases for detailed analysis of their optical properties. The selection criteria for each case were as follows: Case 1, the ozone case, with 1) the concentration of $O_3 > 100$ ppb, 2) the concentration of $[NO_3^-] > 0.6$ μg/m^3, 3) wind speed < 3 m/s, and 4) consecutive duration > 6 h (red shading in Figure 1); Case 2, the transport case with 1) wind direction $>270^o$, 2) wind speed > 4 m/s, and 3) consecutive duration > 6 h (blue shading in Figure 1); and Case 3, the combustion case, with 1) the concentration of $[K^+] > 0.2$ μg/m^3, and 2) consecutive duration > 6 h (yellow shading in Figure 1).

Meanwhile, the HYSPLIT 24-h air mass backward trajectories indicate that during Case 1, air masses predominantly originated from areas close to the sampling site. Combined with low wind speeds (< 3 m/s), meteorological conditions limited atmospheric dispersion, promoting ozone accumulation and secondary pollutant formation (Figure S5). In Case 2, the air mass trajectories were from the inland region, with strong wind speeds that facilitated the transport of pollutants to the sampling site. For Case 3, the air mass trajectories also originated from the interior region but were associated with lower wind speeds than in Case 2.
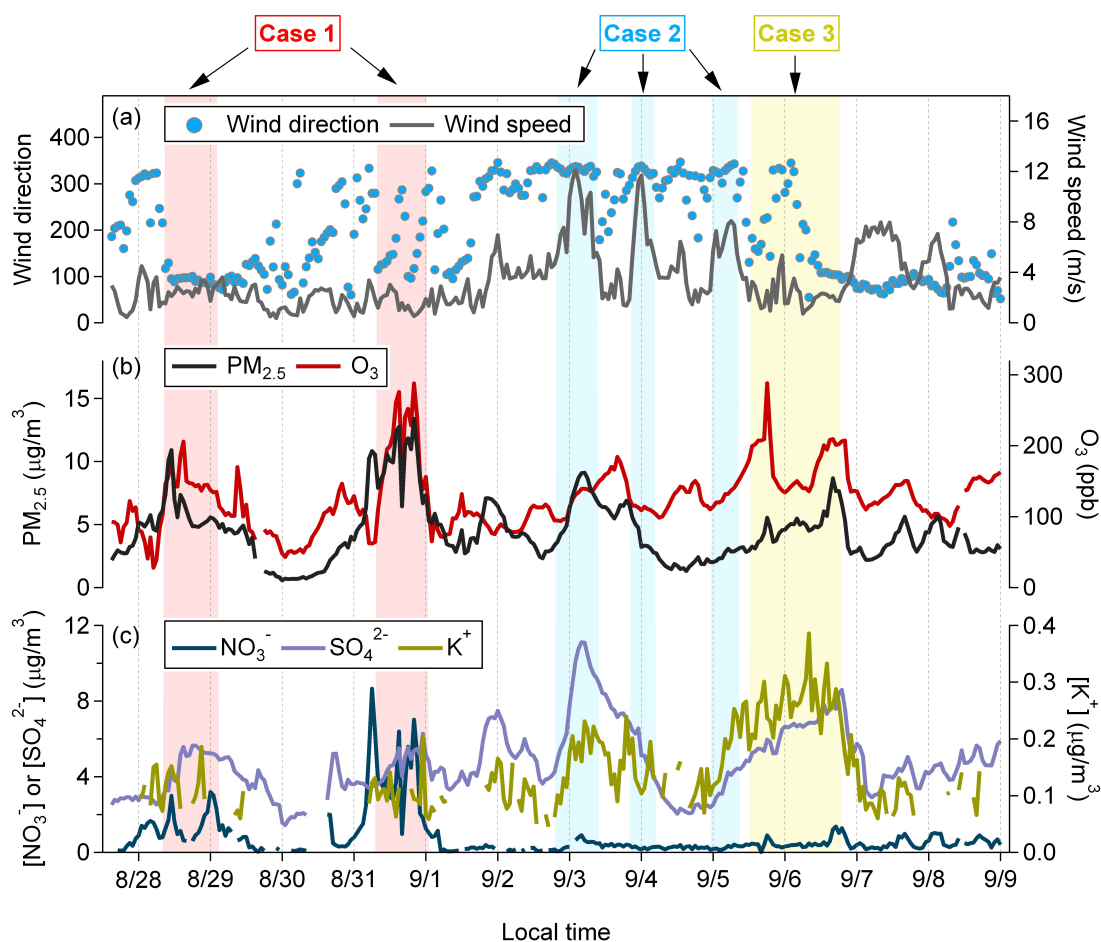
Figure 1. Time series of wind direction and wind speed at the sampling site (a), the concentration of $PM_{2.5}$ and O_3 (b), and chemical composition detected by the MARGA (NO_3^-, SO_4^{2-}, and K^+, d). The colored shadows denote the sampling time for the studied cases (red shading for ozone Case 1, blue shading for transport Case 2, and yellow shading for combustion Case 3).

Polar plots of wind direction, wind speed, and $MAC_{BrC,370}$ were further analyzed for Case 1–3 (Figure 2). In Case 1, the average wind speed was 2.06 m/s, with pollution mainly from local sources (Figure 2a). During Case 1, the average $PM_{2.5}$ concentration was 8.05 ± 2.67 µg/m^3, and the average $MAC_{BrC,370}$ was 1.25 ± 0.56 m^2/g (Figure 2d). For Case 2, the wind primarily came from the northwest, passing over the peninsula, with an average wind speed of 7.81 m/s (Figure 2b). The average $PM_{2.5}$ concentration and $MAC_{BrC,370}$ for Case 2 were 4.87 ± 2.36 µg/m^3 and 2.68 ± 0.30 m^2/g, respectively. In Case 3, the wind speed averaged 2.19 m/s, with erratic wind directions

13

299   (Figure 2c). The average $PM_{2.5}$ concentration and $MAC_{BrC,370}$ for Case 3 were 5.05 ± 1.32 µg/m^3

300   and 3.42 ± 0.41 m^2/g, respectively.

301   Among the three cases, although the average $PM_{2.5}$ concentration in Case 1 was the highest, its

302    $MAC_{BrC,370}$ was the lowest, indicating that the light-absorbing ability of BrC in this high-ozone

303   scenario was relatively weak. The low wind speed in Case 1 limited the influx of transported

304   pollutants. High concentrations of ozone and $[NO_3^-]$ indicated that the aerosols in Case 1 were

305   primarily secondary and highly aged. However, Case 3, characterized by a high concentration of

306   potassium and identified as a plume from combustion sources, had the highest $MAC_{BrC,370}$ in our

307   observations, indicating the strongest light-absorbing ability of combusted BrC among the cases.

308   In real-world atmospheric environments, BrC aerosols often originate from a mixture of sources,

309   and complete source separation is rarely achievable in field studies. While our case-based

310   framework aimed to identify periods with a dominant emission influence, we acknowledge that

311   source mixing may still occur and introduce variability in the retrieved optical parameters. As such,

312   the reported MAC and AAE values should be interpreted as reflecting source-dominant conditions

313   rather than pure-source characteristics. Nevertheless, the clear contrasts in chemical composition

314   and optical responses across cases suggest that dominant sources exert a meaningful influence on

315   BrC absorption. This reinforces the relevance of our findings for understanding BrC behavior

316   under realistic ambient conditions, despite the limitations of bulk sampling and complex source
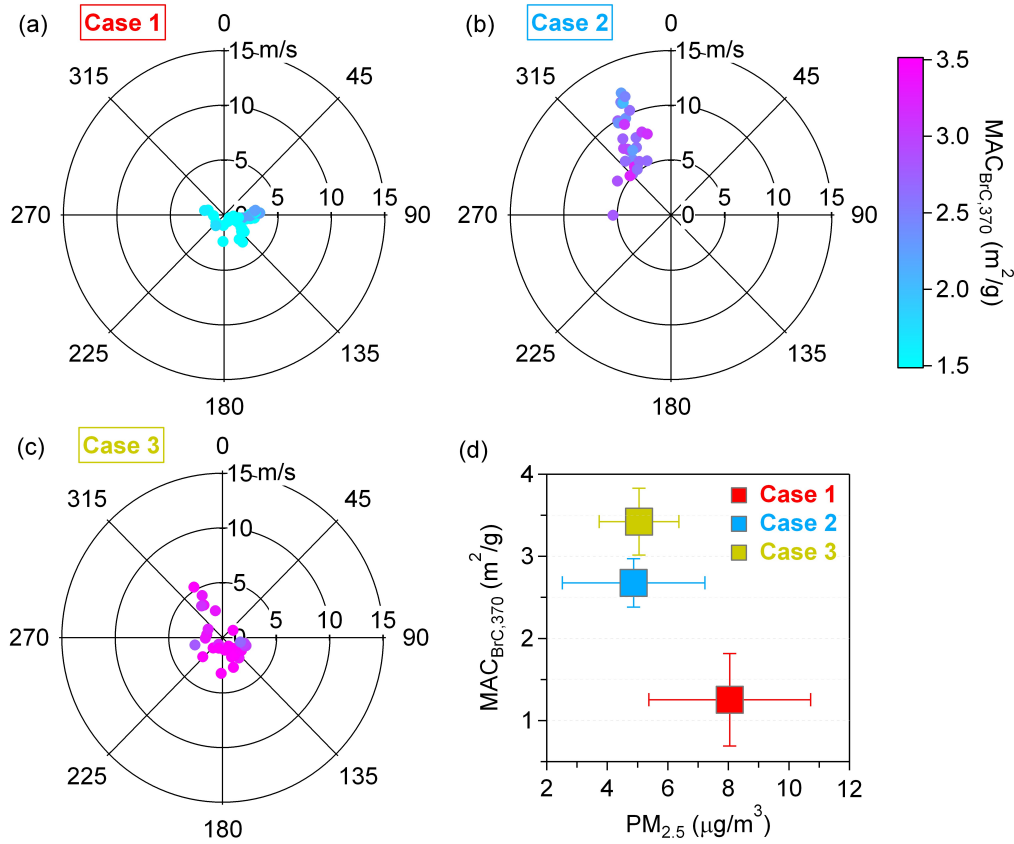
317   environments.

Figure 2. (a–c) Polar plots and $MAC_{BrC,370}$ values for Case 1–3. The radius and color represent the $MAC_{BrC,370}$ values in the downwind direction at specific wind speeds. The color scale denotes the values of $MAC_{BrC,370}$. (d) The mean $MAC_{BrC,370}$ values and mean $PM_{2.5}$ values for Case 1–3. Error bars denote a standard deviation.

3.2 Effects of different aerosol sources on the MAC

By compiling BrC light-absorption measurements reported in 20 studies, Saleh et al. classified BrC into four classes (Saleh, 2020), each with characteristic $MAC_{BrC,550}$ and AAE values: very weakly absorbing (VW-BrC, $MAC_{BrC,550}$ of 1.3×10^{-3}–1.3×10^{-2}, AAE of 7–10), weakly absorbing (W-BrC, $MAC_{BrC,550}$ of 1.3×10^{-2}–0.13, AAE of 5–8), moderately absorbing (M-BrC, $MAC_{BrC,550}$ of 0.13–1.3, AAE of 2.5–5), and strongly absorbing (S-BrC, $MAC_{BrC,550}$ >1.3, AAE of 1.5–2.5). The optical properties defining these BrC classes are expected to be associated with their corresponding physicochemical properties, such as molecular size, volatility, and solubility. In this

15

study, the AAE values for both online measurements of BrC and filter-based offline measurements of WSOC were calculated in the wavelength range of 370 nm to 550 nm, referred to as $AAE_{370-550}$.

For online measurements of BrC, the optical results show an approximately linear correlation. In Case 1, results fall into both the W-BrC and M-BrC categories, whereas results for Case 2 and Case 3 fall primarily into the M-BrC category (Figure 3a). In Case 1, where the ozone concentration is high, BrC shows weaker light-absorbing ability and stronger wavelength dependence compared to Cases 2 & 3. BrC in Case 3 exhibits a high light-absorbing ability with low wavelength dependence. For Case 2, a portion of the optical results overlaps with those from Case 3, possibly due to the transported air mass originating from a similar source as in Case 3.

For the filter-based offline measurements of WSOC, the trend of $AAE_{370-550,WSOC}$ and $MAC_{WSOC,550}$ is consistent with the online results, showing an inverse correlation (Figure 3b). The sample in Case 1 shows the highest wavelength dependence and the lowest light-absorbing ability of WSOC. It's worth noting that although the ozone concentration was also high during Case 3, its optical results did not exhibit the same high wavelength dependence as observed in Case 1. The possible reason could be that primary WSOC produced by combustion has stronger light absorption, which dominated the optical behavior of WSOC during Case 3.

The offline MAC values based on WSOC extractions do not account for Mie scattering effects due to the lack of particle-phase interactions in liquid measurements(Liu et al., 2013;Zeng et al., 2020). Moreover, because particle size distribution and particle mixing state information were not available during the sampling period, Mie model corrections were not be performed in this study. Therefore, direct quantitative comparisons between offline and online MAC values may involve uncertainties. Nevertheless, while the absolute MAC values from the two methods are not directly comparable, the observed trends between the two approaches are generally consistent. This consistency provides additional confidence in the robustness of the observed variations in BrC optical properties across different cases.

356   Saleh et al. suggested that VW-BrC primarily originates from secondary BrC, W-BrC mainly

357   comes from smoldering BrC, and M-BrC is mainly associated with high-temperature BrC (Saleh,

358   2020). However, in our observations, we found that Case 1, which we consider to be dominated

359   by secondary BrC, still falls within the W-BrC or even M-BrC regions for both online airborne

360   measurements and filter-based offline analysis. Possible reasons could be: 1) Unlike laboratory

361   studies, field environments have greater diversity and uncertainty in BrC sources, and 2)

362   differences in measurement methods may lead to variations in the results (Bond and Bergstrom,

363   2006;Saleh, 2020). Although the results for Case 2 fall solely within the S-BrC category, we

364   believe that particles during this period are transported from inland urban areas, where the sources

365   are more complex, including contributions from traffic emissions, industrial combustion,

366   secondary sources, etc.

367   The optical properties of BrC can be affected by atmospheric aging processes such as

368   photochemical bleaching and secondary browning (Zhao et al., 2015). Previous studies have

369   demonstrated that such transformations can occur over timescales of several hours to one day,

370   depending on oxidant levels, radiation intensity, and humidity (Forrister et al., 2015;Washenfelder

371   et al., 2015). In this study, although we did not explicitly isolate aging effects, back-trajectory and

372   chemical evidence suggest that the BrC observed was predominantly regionally influenced, with

373   estimated transport times generally within this aging-relevant range. Therefore, the reported MAC
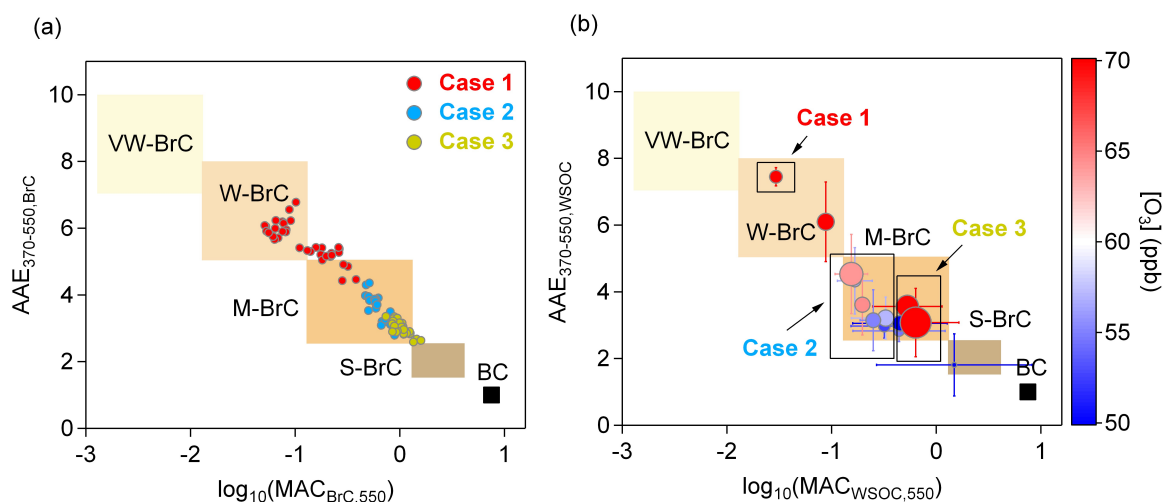
374   and AAE values likely represent moderately aged BrC.

Figure 3. Optical-based BrC classification scheme (Saleh, 2020) in the $\log_{10}(MAC_{550})$ vs. $AAE_{370-550}$ space for (a) BrC and (b) WSOC. The shaded areas represent very weakly absorbing BrC (VW-BrC), weakly absorbing BrC (W-BrC), moderately absorbing BrC (M-BrC), and strongly absorbing BrC (S-BrC). BC is also shown for reference (Bond and Bergstrom, 2006). The scatters in (a) correspond to the online results of Case 1–3. The scatters in (b) correspond to the filter-based results during the sampling period with each scatter representing a filter in 24 h sampling duration. The color scale in (b) denotes the ozone concentration in ppb. The size of scatters in (b) denotes the concentration of K^+ detected by the MARGA. Error bars denote the standard deviation of the results for three repeated experiments.

3.3 Chemical characterization of BrC molecules

The water-soluble organic carbon (WSOC) species were ionized using ESI+ and ESI- ionization modes to detect the organic compounds. The identified molecules were categorized into groups based on atom composition: CHO, CHON, CHOS, and CHONS. The van Krevelen (VK) diagram is a widely used graphical method that plots H/C ratios against O/C ratios in molecular formulas to qualitatively identify the major chemical species in WSOC (Kim et al., 2003). In this study, the VK space is divided into seven regions based on previous studies: (1) lipid-like (O/C = 0–0.3, H/C = 1.5–2.0), (2) aliphatic/protein-like (O/C = 0.3–0.67, H/C = 1.5–2.2), (3) carbohydrate-like (O/C

18

393　= 0.67–1.2, H/C = 1.5–2.4), (4) unsaturated hydrocarbons (O/C = 0–0.1, H/C = 0.7–1.5), (5)

394　lignins/carboxylic-rich alicyclic-molecule-like (CRAM) (O/C = 0.1–0.67, H/C = 0.7–1.5), (6)

395　tannin-like (O/C = 0.67–1.2, H/C = 0.5–1.5), and (7) condensed aromatics (O/C = 0–0.67, H/C =

396　0.2–0.7) (Feng et al., 2016;Ohno et al., 2010;Zeng et al., 2024). The sizes of scatters in Figure 4

397　are proportional to the absorbance.

398　　For each case, filters were selected to coincide with the core pollution periods, characterized by

399　stable meteorological conditions and elevated pollutant concentrations. Although the number of

400　samples was limited, the chemical results are considered reasonably representative of the dominant

401　source influences during these periods. In Case 1, CHO compounds, which account for 36.5% of

402　the absorbance, are the most abundant form of BrC. These CHO compounds likely contain

403　carboxyl or hydroxyl functional groups. The light-absorbing CHO compounds may originate from

404　biomass burning smoke (Desyaterik et al., 2013;Chen et al., 2022a;Zhou et al., 2022;Chen et al.,

405　2023) and have also been detected in water-soluble organic carbon (WSOC) and cloud water

406　(Bianco et al., 2018;Kourtchev et al., 2016). Secondary CHO compounds, including typical dimers

407　of α-pinene and diterpenoid derivatives, have also been detected in previous studies (Kourtchev et

408　al., 2014;Kristensen et al., 2014;Gómez-González et al., 2012). The CHOS group in Case 2

409　contributes the highest relative absorbance (29.5%). The CHOS compounds are considered to

410　contain long aliphatic carbon chains with low aromaticity and are typically derived from

411　anthropogenic emissions, such as diesel vehicles (Tao et al., 2014), coal combustions (Song et al.,

412　2019), and vessels (Cui et al., 2019). The CHON group in Case 3 exhibits the highest relative

413　absorbance (43.2%). It's worth noting that, although CHON is not the most abundant group in

414　terms of molecular abundance, its relative absorbance is the highest, suggesting that CHON

415　compounds have a strong molecular absorption capacity. The CHON compounds have been found

416　to be mainly derived from biomass burning species, such as nitrophenols, nitrocatechols,

417　nitroguaiacols, etc. (Kourtchev et al., 2015;Zhang et al., 2013;Song et al., 2018). Several CHON

418　species consistent with indole-derived structures, including isatin ($C_8H_5NO_2$) and nitroindole

419　($C_8H_6N_2O_2$, $C_8H_7NO_4$) were detected in the mass spectra. The identification of these compounds

supports the attribution of the observed BrC to biomass burning sources (Baboomian et al., 2023;Chen et al., 2023;Mayorga et al., 2022;Jiang et al., 2019;Montoya-Aguilera et al., 2017), and highlights the complexity of nitrogen-containing brown carbon species in ambient aerosols. To provide a clearer overview of the molecular-level characteristics of BrC identified in this study, we summarized the major light-absorbing organic compounds and structures detected in the field samples in Table S1. We further conducted a correlation analysis between the relative absorbance of CHON and the MAC of WSOC throughout the whole sampling period, finding that as the relative absorbance of CHON increases, the MAC of BrC also becomes larger (Figure S7). The measurement of chemical molecules provides support for the results corresponding to our optical observations in different cases.

In the VK diagram, aliphatics, lignins, and carbohydrates dominate in all three cases. In Case 3, WSOC shows a higher proportion of absorbance from lignins, which are commonly attributed to biomolecules and biomass burning species (Kitanovski et al., 2014). The differences in the chemical molecular compositions of BrC across the different cases during our observations led to variations in the light absorption of organic matter.
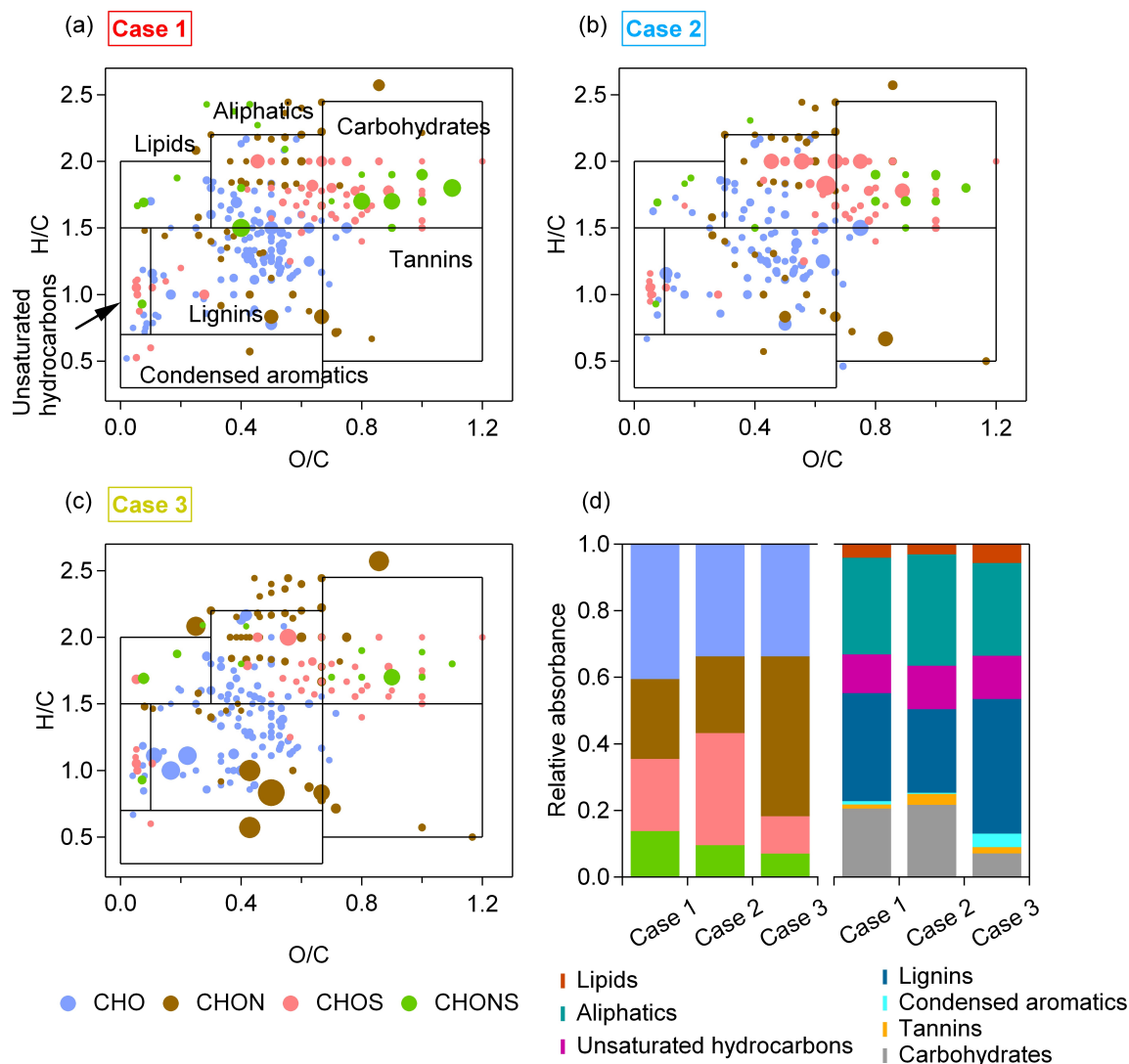
Figure 4. Sources of WSOC formula categories. (a–c) Van Krevelen plots for Case 1–3. Different formula categories are color coded. The sizes of scatters are proportional to the absorbance. The boxes indicate the classifications of various chemical species. (d) Relative absorbance of different formula categories (CHO, CHON, CHOS, and CHONS), and of different chemical species (lipids, aliphatics, unsaturated hydrocarbons, lignins, condensed aromatics, tannins, and carbohydrates).

4 CONCLUSIONS

The diverse chemical composition of atmospheric light-absorbing organics leads to distinct optical properties for BrC from different sources. However, studies on the optical properties of multi-

444   source atmospheric BrC, particularly those based on field observations, remain limited. The main

445   challenge arises from the complex and variable ambient conditions, which complicate the accurate

446   identification of BrC from different sources. In this study, a sampling site located away from urban

447   areas was selected, providing a more favorable environment for distinguishing BrC from primary

448   and secondary sources. Through field measurements, we independently identified various BrC

449   sources, including secondary BrC from ozone oxidation, primary BrC transported from urban

450   sources, and typical combustion-derived BrC. We found that the MAC of BrC varied by source,

451   with secondary BrC from ozone pollution being the least absorbing but exhibiting the highest AAE,

452   while BrC from biomass combustion was the most absorbing with the lowest AAE.

453   A key challenge in representing BrC absorption in climate models is its significant variability

454   in light absorption capacity. The representation of BrC absorption in climate models could be

455   improved by differentiating BrC sources or categorizing BrC into distinct optical ranges. Our direct

456   field measurements contribute to a better understanding of the optical properties of multi-source

457   BrC.

458

References:

Al Fischer, D., and Smith, G. D.: A portable, four-wavelength, single-cell photoacoustic spectrometer for ambient aerosol absorption, Aerosol Sci. Technol., 52, 393-406, 10.1080/02786826.2017.1413231, 2018.

Anderson, T. L., and Ogren, J. A.: Determining aerosol radiative properties using the TSI 3563 integrating nephelometer, Aerosol Sci. Technol., 29, 57-69, 10.1080/02786829808965551, 1998.

Arnott, W. P., Moosmüller, H., Rogers, C. F., Jin, T., and Bruch, R.: Photoacoustic spectrometer for measuring light absorption by aerosol: instrument description, Atmos. Environ., 33, 2845-2852, 1998.

Baboomian, V. J., He, Q. F., Montoya-Aguilera, J., Ali, N., Fleming, L. T., Lin, P., Laskin, A., Laskin, J., Rudich, Y., and Nizkorodov, S. A.: Light absorption and scattering properties of indole secondary organic aerosol prepared under various oxidant and relative humidity conditions, Aerosol Sci. Technol., 57, 532-545, 10.1080/02786826.2023.2193235, 2023.

Bianco, A., Deguillaume, L., Vaitilingom, M., Nicol, E., Baray, J. L., Chaumerliac, N., and Bridoux, M.: Molecular characterization of cloud water samples collected at the Puy de Dome (France) by fourier transform ion cyclotron resonance mass spectrometry, Environ. Sci. Technol., 52, 10275-10285, 10.1021/acs.est.8b01964, 2018.

Bond, T. C., and Bergstrom, R. W.: Light absorption by carbonaceous particles: An investigative review, Aerosol Sci. Technol., 40, 27-67, 10.1080/02786820500421521, 2006.

Bond, T. C., Covert, D. S., and Müller, T.: Truncation and angular-scattering corrections for absorbing aerosol in the TSI 3563 nephelometer, Aerosol Sci. Technol., 43, 866-871, 10.1080/02786820902998373, 2009.

Bones, D. L., Henricksen, D. K., Mang, S. A., Gonsior, M., Bateman, A. P., Nguyen, T. B., Cooper, W. J., and Nizkorodov, S. A.: Appearance of strong absorbers and fluorophores in limonene-O3 secondary organic aerosol due to NH4+-mediated chemical aging over long time scales, J. Geophys. Res. Atmos., 115, 10.1029/2009jd012864, 2010.

Cappa, C. D., Lack, D. A., Burkholder, J. B., and Ravishankara, A. R.: Bias in filter-based aerosol light absorption measurements due to organic aerosol loading: Evidence from laboratory measurements, Aerosol Sci. Technol., 42, 1022-1032, 10.1080/02786820802389285, 2008.

Chang, J. L., and Thompson, J. E.: Characterization of colored products formed during irradiation of aqueous solutions containing H2O2 and phenolic compounds, Atmos. Environ., 44, 541-551, 10.1016/j.atmosenv.2009.10.042, 2010.

Chen, J., Wenger, J. C., and Venables, D. S.: Near-ultraviolet absorption cross sections of nitrophenols and their potential influence on tropospheric oxidation capacity, J. Phys. Chem. A, 115, 12235-12242, 10.1021/jp206929r, 2011.

Chen, K. P., Mayorga, R., Raeofy, N., Lum, M., Woods, M., Bahreini, R., Zhang, H. F., and Lin, Y. H.: Effects of nitrate radical levels and pre-existing particles on secondary brown carbon formation from nighttime oxidation of furan, ACS Earth Space Chem., 6, 2709-2721, 2709-2721, 10.1021/acsearthspacechem.2c00244, 2022a.

Chen, K. P., Raeofy, N., Lum, M., Mayorga, R., Woods, M., Bahreini, R., Zhang, H. F., and Lin, Y. H.: Solvent effects on chemical composition and optical properties of extracted secondary brown carbon constituents, Aerosol Sci. Technol., 56, 917-930, 10.1080/02786826.2022.2100734, 2022b.

Chen, K. P., Mayorga, R., Hamilton, C., Bahreini, R., Zhang, H. F., and Lin, Y. H.: Contribution of carbonyl chromophores in secondary brown carbon from nighttime oxidation of unsaturated heterocyclic volatile organic compounds, Environ. Sci. Technol., 57, 20085-20096, 10.1021/acs.est.3c08872, 2023.

Chen, Y., and Bond, T. C.: Light absorption by organic carbon from wood combustion, Atmos. Chem. Phys., 10, 1773-1787, 2010.

Claeys, M., Vermeylen, R., Yasmeen, F., Gómez-González, Y., Chi, X. G., Maenhaut, W., Mészáros, T., and Salma, I.: Chemical characterisation of humic-like substances from urban, rural and tropical biomass burning environments using liquid chromatography with UV/vis photodiode array detection and electrospray ionisation mass spectrometry, Environ. Chem., 9, 273-284, 10.1071/en11163, 2012.

Cui, M., Li, C., Chen, Y. J., Zhang, F., Li, J., Jiang, B., Mo, Y. Z., Li, J., Yan, C. Q., Zheng, M., Xie, Z. Y., Zhang, G., and Zheng, J. Y.: Molecular characterization of polar organic aerosol constituents in off-road engine emissions using Fourier transform ion cyclotron resonance mass spectrometry (FT-ICR MS): implications for source apportionment, Atmos. Chem. Phys., 19, 13945-13956, 10.5194/acp-19-13945-2019, 2019.

Cui, Y., Chen, K., Zhang, H., Lin, Y.-H., and Bahreini, R.: Chemical composition and optical properties of secondary organic aerosol from photooxidation of volatile organic compound mixtures, ACS ES&T Air, 1, 247-258, 10.1021/acsestair.3c00041, 2024.

Dalton, A. B., Wingen, L. M., and Nizkorodov, S. A.: Isomeric identification of the nitroindole chromophore in indole, ACS Phys. Chem. Au, 4, 568-574, 10.1021/acsphyschemau.4c00044, 2024.

Desyaterik, Y., Sun, Y., Shen, X. H., Lee, T. Y., Wang, X. F., Wang, T., and Collett, J. L.: Speciation of "brown" carbon in cloud water impacted by agricultural biomass burning in eastern China, J. Geophys. Res. Atmos., 118, 7389-7399, 10.1002/jgrd.50561, 2013.

Feng, L., Xu, J. Z., Kang, S. C., Li, X. F., Li, Y., Jiang, B., and Shi, Q.: Chemical composition of microbe-derived dissolved organic matter in cryoconite in Tibetan Plateau glaciers: Insights from fourier transform ion cyclotron resonance mass spectrometry analysis, Environ. Sci.

549   Technol., 50, 13215-13223, 10.1021/acs.est.6b03971, 2016.

550 Flores, J. M., Zhao, D. F., Segev, L., Schlag, P., Kiendler-Scharr, A., Fuchs, H., Watne, A. K.,
551   Bluvshtein, N., Mentel, T. F., Hallquist, M., and Rudich, Y.: Evolution of the complex refractive
552   index in the UV spectral region in ageing secondary organic aerosol, Atmos. Chem. Phys., 14,
553   5793-5806, 10.5194/acp-14-5793-2014, 2014.

554 Forrister, H., Liu, J., Scheuer, E., Dibb, J., Ziemba, L., Thornhill, K. L., Anderson, B., Diskin, G.,
555   Perring, A. E., Schwarz, J. P., Campuzano-Jost, P., Day, D. A., Palm, B. B., Jimenez, J. L., Nenes,
556   A., and Weber, R. J.: Evolution of brown carbon in wildfire plumes, Geophys. Res. Lett., 42,
557   4623-4630, 10.1002/2015gl063897, 2015.

558 Gómez-González, Y., Wang, W., Vermeylen, R., Chi, X., Neirynck, J., Janssens, I. A., Maenhaut,
559   W., and Claeys, M.: Chemical characterisation of atmospheric aerosols during a 2007 summer
560   field campaign at Brasschaat, Belgium: sources and source processes of biogenic secondary
561   organic aerosol, Atmos. Chem. Phys., 12, 125-138, 10.5194/acp-12-125-2012, 2012.

562 Haynes, J. P., Miller, K. E., and Majestic, B. J.: Investigation into photoinduced auto-oxidation of
563   polycyclic aromatic hydrocarbons resulting in brown carbon production, Environ. Sci. Technol.,
564   53, 682-691, 10.1021/acs.est.8b05704, 2019.

565 Hecobian, A., Zhang, X., Zheng, M., Frank, N., Edgerton, E., and Weber, R.: Water-soluble organic
566   aerosol material and the light-absorption characteristics of aqueous extracts measured over the
567   Southeastern United States, Atmos. Chem. Phys., 10, 5965-5977, 10.5194/acp-10-5965-2010,
568   2010.

569 Jiang, H. H., Frie, A. L., Lavi, A., Chen, J. Y., Zhang, H. F., Bahreini, R., and Lin, Y. H.: Brown
570   carbon formation from nighttime chemistry of unsaturated heterocyclic volatile organic
571   compounds, Environ. Sci. Technol. Lett., 6, 184-190, 10.1021/acs.estlett.9b00017, 2019.

572 Kim, S., Kramer, R. W., and Hatcher, P. G.: Graphical method for analysis of ultrahigh-resolution
573   broadband mass spectra of natural organic matter, the van Krevelen diagram, Anal. Chem., 75,
574   5336-5344, 10.1021/ac034415p, 2003.

575 Kitanovski, Z., Cusak, A., Grgic, I., and Claeys, M.: Chemical characterization of the main
576   products formed through aqueous-phase photonitration of guaiacol, Atmos. Meas. Tech., 7,
577   2457-2470, 10.5194/amt-7-2457-2014, 2014.

578 Kourtchev, I., Fuller, S. J., Giorio, C., Healy, R. M., Wilson, E., O'Connor, I., Wenger, J. C.,
579   McLeod, M., Aalto, J., Ruuskanen, T. M., Maenhaut, W., Jones, R., Venables, D. S., Sodeau, J.
580   R., Kulmala, M., and Kalberer, M.: Molecular composition of biogenic secondary organic
581   aerosols using ultrahigh-resolution mass spectrometry: comparing laboratory and field studies,
582   Atmos. Chem. Phys., 14, 2155-2167, 10.5194/acp-14-2155-2014, 2014.

583 Kourtchev, I., Doussin, J. F., Giorio, C., Mahon, B., Wilson, E. M., Maurin, N., Pangui, E.,
584   Venables, D. S., Wenger, J. C., and Kalberer, M.: Molecular composition of fresh and aged

secondary organic aerosol from a mixture of biogenic volatile compounds: a high-resolution mass spectrometry study, Atmos. Chem. Phys., 15, 5683-5695, 10.5194/acp-15-5683-2015, 2015.

Kourtchev, I., Godoi, R. H. M., Connors, S., Levine, J. G., Archibald, A. T., Godoi, A. F. L., Paralovo, S. L., Barbosa, C. G. G., Souza, R. A. F., Manzi, A. O., Seco, R., Sjostedt, S., Park, J. H., Guenther, A., Kim, S., Smith, J., Martin, S. T., and Kalberer, M.: Molecular composition of organic aerosols in central Amazonia: an ultra-high-resolution mass spectrometry study, Atmos. Chem. Phys., 16, 11899-11913, 10.5194/acp-16-11899-2016, 2016.

Kristensen, K., Cui, T., Zhang, H., Gold, A., Glasius, M., and Surratt, J. D.: Dimers in α-pinene secondary organic aerosol: effect of hydroxyl radical, ozone, relative humidity and aerosol acidity, Atmos. Chem. Phys., 14, 4201-4218, 10.5194/acp-14-4201-2014, 2014.

Kruve, A.: Semi-quantitative non-target analysis of water with liquid chromatography/high-resolution mass spectrometry: How far are we?, Rapid Commun. Mass Sp., 33, 54-63, 10.1002/rcm.8208, 2019.

Kumar, N. K., Corbin, J. C., Bruns, E. A., Massabó, D., Slowik, J. G., Drinovec, L., Mocnik, G., Prati, P., Vlachou, A., Baltensperger, U., Gysel, M., El-Haddad, I., and Prévôt, A. S. H.: Production of particulate brown carbon during atmospheric aging of residential wood-burning emissions, Atmos. Chem. Phys., 18, 17843-17861, 10.5194/acp-18-17843-2018, 2018.

Lack, D. A., Cappa, C. D., Covert, D. S., Baynard, T., Massoli, P., Sierau, B., Bates, T. S., Quinn, P. K., Lovejoy, E. R., and Ravishankara, A. R.: Bias in filter-based aerosol light absorption measurements due to organic aerosol loading: Evidence from ambient measurements, Aerosol Sci. Technol., 42, 1033-1041, 10.1080/02786820802389277, 2008.

Lambe, A. T., Cappa, C. D., Massoli, P., Onasch, T. B., Forestieri, S. D., Martin, A. T., Cummings, M. J., Croasdale, D. R., Brune, W. H., Worsnop, D. R., and Davidovits, P.: Relationship between oxidation level and optical properties of secondary organic aerosol, Environ. Sci. Technol., 47, 6349-6357, 10.1021/es401043j, 2013.

Laskin, A., Laskin, J., and Nizkorodov, S. A.: Chemistry of atmospheric brown carbon, Chem. Rev., 10.1021/cr5006167, 2015.

Lewis, K., Arnott, W. P., Moosmuller, H., and Wold, C. E.: Strong spectral variation of biomass smoke light absorption and single scattering albedo observed with a novel dual-wavelength photoacoustic instrument, J. Geophys. Res. Atmos., 113, 10.1029/2007jd009699, 2008.

Li, C. L., He, Q. F., Hettiyadura, A. P. S., Käfer, U., Shmul, G., Meidan, D., Zimmermann, R., Brown, S. S., George, C., Laskin, A., and Rudich, Y.: Formation of secondary brown carbon in biomass burning aerosol proxies through NO3 radical reactions, Environ. Sci. Technol., 54, 1395-1405, 10.1021/acs.est.9b05641, 2020.

Li, K., Wang, W. G., Ge, M. F., Li, J. J., and Wang, D.: Optical properties of secondary organic

aerosols generated by photooxidation of aromatic hydrocarbons, Sci. Rep., 4, 10.1038/srep04922, 2014.

Liu, J., Bergin, M., Guo, H., King, L., Kotra, N., Edgerton, E., and Weber, R. J.: Size-resolved measurements of brown carbon in water and methanol extracts and estimates of their contribution to ambient fine-particle light absorption, Atmos. Chem. Phys., 13, 12389-12404, 10.5194/acp-13-12389-2013, 2013.

Massabò, D., Caponi, L., Bove, M. C., and Prati, P.: Brown carbon and thermal-optical analysis: A correction based on optical multi-wavelength apportionment of atmospheric aerosols, Atmos. Environ., 125, 119-125, 10.1016/j.atmosenv.2015.11.011, 2016.

Massoli, P., Kebabian, P. L., Onasch, T. B., Hills, F. B., and Freedman, A.: Aerosol light extinction measurements by cavity attenuated phase shift (CAPS) spectroscopy: Laboratory validation and field deployment of a compact aerosol particle extinction monitor, Aerosol Sci. Technol., 44, 428-435, 10.1080/02786821003716599, 2010.

Mayorga, R., Chen, K. P., Raeofy, N., Woods, M., Lum, M., Zhao, Z. X., Zhang, W., Bahreini, R., Lin, Y. H., and Zhang, H. F.: Chemical structure regulates the formation of secondary organic aerosol and brown carbon in nitrate radical oxidation of pyrroles and methylpyrroles, Environ. Sci. Technol., 56, 7761-7770, 10.1021/acs.est.2c02345, 2022.

Moise, T., Flores, J. M., and Rudich, Y.: Optical properties of secondary organic aerosols and their changes by chemical processes, Chem. Rev., 10.1021/cr5005259, 2015.

Montoya-Aguilera, J., Horne, J. R., Hinks, M. L., Fleming, L. T., Perraud, V., Lin, P., Laskin, A., Laskin, J., Dabdub, D., and Nizkorodov, S. A.: Secondary organic aerosol from atmospheric photooxidation of indole, Atmos. Chem. Phys., 17, 11605-11621, 10.5194/acp-17-11605-2017, 2017.

Nozière, B., Dziedzic, P., and Córdova, A.: Products and kinetics of the liquid-phase reaction of glyoxal catalyzed by ammonium ions (NH4(+)), J. Phys. Chem. A, 113, 231-237, 10.1021/jp8078293, 2009.

Ohno, T., He, Z. Q., Sleighter, R. L., Honeycutt, C. W., and Hatcher, P. G.: Ultrahigh resolution mass spectrometry and indicator species analysis to identify marker components of soil- and plant biomass-derived organic matter fractions, Environ. Sci. Technol., 44, 8594-8600, 10.1021/es101089t, 2010.

Olson, M. R., Garcia, M. V., Robinson, M. A., Van Rooy, P., Dietenberger, M. A., Bergin, M., and Schauer, J. J.: Investigation of black and brown carbon multiple-wavelength-dependent light absorption from biomass and fossil fuel combustion source emissions, J. Geophys. Res. Atmos., 120, 6682-6697, 10.1002/2014jd022970, 2015.

Pani, S. K., Lin, N. H., Griffith, S. M., Chantara, S., Lee, C. T., Thepnuan, D., and Tsai, Y.: Brown carbon light absorption over an urban environment in northern peninsular Southeast Asia,

657   Environ. Pollut., 276, 10.1016/j.envpol.2021.116735, 2021.

658   Petzold, A., Schloesser, H., Sheridan, P. J., Arnott, W. P., Ogren, J. A., and Virkkula, A.: Evaluation
659   of multiangle absorption photometry for measuring aerosol light absorption, Aerosol Sci.
660   Technol., 39, 40-51, 10.1080/027868290901945, 2005.

661   Rathod, T. D., Sahu, S. K., Tiwari, M., Bhangare, R. C., and Ajmal, P. Y.: Optical properties of
662   water soluble and organic soluble carbonaceous aerosols at an urban location in India, Atmos.
663   Pollut. Res., 15, 10.1016/j.apr.2023.101956, 2024.

664   Riziq, A. A., Erlick, C., Dinar, E., and Rudich, Y.: Optical properties of absorbing and non-
665   absorbing aerosols retrieved by cavity ring down (CRD) spectroscopy, Atmos. Chem. Phys., 7,
666   1523-1536, 2007.

667   Saleh, R., Robinson, E. S., Tkacik, D. S., Ahern, A. T., Liu, S., Aiken, A. C., Sullivan, R. C., Presto,
668   A. A., Dubey, M. K., Yokelson, R. J., Donahue, N. M., and Robinson, A. L.: Brownness of
669   organics in aerosols from biomass burning linked to their black carbon content, Nat. Geosci., 7,
670   647-650, 10.1038/ngeo2220, 2014.

671   Saleh, R., Cheng, Z. Z., and Atwi, K.: The brown-black continuum of light-absorbing combustion
672   aerosols, Environ. Sci. Technol. Lett., 5, 508-513, 10.1021/acs.estlett.8b00305, 2018.

673   Saleh, R.: From measurements to models: Toward accurate representation of brown carbon in
674   climate calculations, Curr. Pollut. Rep., 6, 90-104, 10.1007/s40726-020-00139-3, 2020.

675   Shapiro, E. L., Szprengiel, J., Sareen, N., Jen, C. N., Giordano, M. R., and McNeill, V. F.: Light-
676   absorbing secondary organic material formed by glyoxal in aqueous aerosol mimics, Atmos.
677   Chem. Phys., 9, 2289-2300, 10.5194/acp-9-2289-2009, 2009.

678   Shetty, N. J., Pandey, A., Baker, S., Hao, W. M., and Chakrabarty, R. K.: Measuring light
679   absorption by freshly emitted organic aerosols: optical artifacts in traditional solvent-extraction-
680   based methods, Atmos. Chem. Phys., 19, 8817-8830, 10.5194/acp-19-8817-2019, 2019.

681   Song, J. Z., Li, M. J., Jiang, B., Wei, S. Y., Fan, X. J., and Peng, P. A.: Molecular characterization
682   of water-soluble humic like substances in smoke particles emitted from combustion of biomass
683   materials and coal using ultrahigh-resolution electrospray ionization fourier transform ion
684   cyclotron resonance mass spectrometry, Environ. Sci. Technol., 52, 2575-2585,
685   10.1021/acs.est.7b06126, 2018.

686   Song, J. Z., Li, M. J., Fan, X. J., Zou, C. L., Zhu, M. B., Jiang, B., Yu, Z. Q., Jia, W. L., Liao, Y.
687   H., and Peng, P. A.: Molecular characterization of water- and methanol-soluble organic
688   compounds emitted from residential coal combustion using ultrahigh-resolution electrospray
689   ionization fourier transform ion cyclotron resonance mass spectrometry, Environ. Sci. Technol.,
690   53, 13607-13617, 10.1021/acs.est.9b04331, 2019.

691   Subramanian, R., Roden, C. A., Boparai, P., and Bond, T. C.: Yellow beads and missing particles:

Trouble ahead for filter-based absorption measurements, Aerosol Sci. Technol., 41, 630-637, 10.1080/02786820701344589, 2007.

Sumlin, B. J., Pandey, A., Walker, M. J., Pattison, R. S., Williams, B. J., and Chakrabarty, R. K.: Atmospheric photooxidation diminishes light absorption by primary brown carbon aerosol from biomass burning, Environ. Sci. Technol. Lett., 4, 540-545, 10.1021/acs.estlett.7b00393, 2017.

Sun, H., Biedermann, L., and Bond, T. C.: Color of brown carbon: A model for ultraviolet and visible light absorption by organic carbon aerosol, Geophys. Res. Lett., 34, 10.1029/2007gl029797, 2007.

Tao, S., Lu, X., Levac, N., Bateman, A. P., Nguyen, T. B., Bones, D. L., Nizkorodov, S. A., Laskin, J., Laskin, A., and Yang, X.: Molecular characterization of organosulfates in organic aerosols from Shanghai and Los Angeles urban areas by nanospray-desorption electrospray ionization high-resolution mass spectrometry, Environ. Sci. Technol., 48, 10993-11001, 10.1021/es5024674, 2014.

Updyke, K. M., Nguyen, T. B., and Nizkorodov, S. A.: Formation of brown carbon via reactions of ammonia with secondary organic aerosols from biogenic and anthropogenic precursors, Atmos. Environ., 63, 22-31, 10.1016/j.atmosenv.2012.09.012, 2012.

Washenfelder, R. A., Attwood, A. R., Brock, C. A., Guo, H., Xu, L., Weber, R. J., Ng, N. L., Allen, H. M., Ayres, B. R., Baumann, K., Cohen, R. C., Draper, D. C., Duffey, K. C., Edgerton, E., Fry, J. L., Hu, W. W., Jimenez, J. L., Palm, B. B., Romer, P., Stone, E. A., Wooldridge, P. J., and Brown, S. S.: Biomass burning dominates brown carbon absorption in the rural southeastern United States, Geophys. Res. Lett., 42, 653-664, 10.1002/2014gl062444, 2015.

Wen, H., Zhou, Y., Xu, X., Wang, T., Chen, Q., Chen, Q., Li, W., Wang, Z., Huang, Z., Zhou, T., Shi, J., Bi, J., Ji, M., and Wang, X.: Water-soluble brown carbon in atmospheric aerosols along the transport pathway of Asian dust: Optical properties, chemical compositions, and potential sources, Sci. Total Environ., 789, 10.1016/j.scitotenv.2021.147971, 2021.

Wong, J. P. S., Nenes, A., and Weber, R. J.: Changes in light absorptivity of molecular weight separated brown carbon due to photolytic aging, Environ. Sci. Technol., 51, 8414-8421, 10.1021/acs.est.7b01739, 2017.

Zarzana, K. J., De Haan, D. O., Freedman, M. A., Hasenkopf, C. A., and Tolbert, M. A.: Optical properties of the products of α-dicarbonyl and amine reactions in simulated cloud droplets, Environ. Sci. Technol., 46, 4845-4851, 10.1021/es2040152, 2012.

Zeng, L. H., Zhang, A. X., Wang, Y. H., Wagner, N. L., Katich, J. M., Schwarz, J. P., Schill, G. P., Brock, C., Froyd, K. D., Murphy, D. M., Williamson, C. J., Kupc, A., Scheuer, E., Dibb, J., and Weber, R. J.: Global measurements of brown carbon and estimated direct radiative effects, Geophys. Res. Lett., 47, 10.1029/2020gl088747, 2020.

Zeng, Y. L., Zhang, A. T., Yang, X., Xing, C. B., Zhai, J. H., Wang, Y. X., Cai, B. H., Shi, S., Zhang,

Y. J., Shen, Z. X., Fu, T. M., Zhu, L., Shen, H. Z., Ye, J. H., and Wang, C.: Internal exposure potential of water-soluble organic molecules in urban PM2.5 evaluated by non-covalent adductome of human serum albumin, Environ. Int., 184, 10.1016/j.envint.2024.108492, 2024.

Zhai, J., Wang, X., Li, J., Xu, T., Chen, H., Yang, X., and Chen, J.: Thermal desorption single particle mass spectrometry of ambient aerosol in Shanghai, Atmos. Environ., 123, 407-414, 10.1016/j.atmosenv.2015.09.001, 2015.

Zhang, A. T., Zeng, Y. L., Yang, X., Zhai, J. H., Wang, Y. X., Xing, C. B., Cai, B. H., Shi, S., Zhang, Y. J., Shen, Z. X., Fu, T. M., Zhu, L., Shen, H. Z., Ye, J. H., and Wang, C.: Organic matrix effect on the molecular light absorption of brown carbon, Geophys. Res. Lett., 50, 10.1029/2023gl106541, 2023.

Zhang, X. L., Lin, Y. H., Surratt, J. D., and Weber, R. J.: Sources, composition and absorption angstrom exponent of light-absorbing organic components in aerosol extracts from the Los Angeles Basin, Environ. Sci. Technol., 47, 3685-3693, 10.1021/es305047b, 2013.

Zhao, R., Lee, A. K. Y., Huang, L., Li, X., Yang, F., and Abbatt, J. P. D.: Photochemical processing of aqueous atmospheric brown carbon, Atmos. Chem. Phys., 15, 6087-6100, 10.5194/acp-15-6087-2015, 2015.

Zhong, M., and Jang, M.: Light absorption coefficient measurement of SOA using a UV-Visible spectrometer connected with an integrating sphere, Atmos. Environ., 45, 4263-4271, 10.1016/j.atmosenv.2011.04.082, 2011.

Zhou, Y., West, C. P., Hettiyadura, A. P. S., Pu, W., Shi, T. L., Niu, X. Y., Wen, H., Cui, J. C., Wang, X., and Laskin, A.: Molecular characterization of water-soluble brown carbon chromophores in snowpack from Northern Xinjiang, China, Environ. Sci. Technol., 56, 4173-4186, 10.1021/acs.est.1c07972, 2022.